



Article

Experimental Investigation of Thermoacoustics and High-Frequency Combustion Dynamics with Band Stop Characteristics in a Pressurized Combustor

Mehmet Kapucu *, Jim B. W. Kok  and Artur K. Pozarlik 

Faculty of Engineering Technology, University of Twente, 7522 NB Enschede, The Netherlands; j.b.w.kok@utwente.nl (J.B.W.K.); a.k.pozarlik@utwente.nl (A.K.P.)

* Correspondence: m.kapucu@utwente.nl

Abstract: In combustor systems, thermoacoustic instabilities may occur and must be avoided for reliable operation. An acoustic network model can be used to predict the eigenfrequencies of the instabilities and the growth rate by incorporating the combustion dynamics with a flame transfer function (FTF). The FTF defines the interconnection between burner aerodynamics and the rate of combustion. In the current study, the method to measure the FTF in a pressurized combustor is explored. A siren unit, mounted in the fuel line, induced a fuel flow excitation of variable amplitude and high maximum frequency. This was performed here for pressurized conditions at 1.5 bar and 3 bar and at a thermal power of 125 kW and 250 kW. In addition to the experimental investigation, a 1-D acoustic network model approach is used. In the model, thermoviscous damping effects and reflection coefficients are incorporated. The model results compare well with experimental data, indicating that the proposed method to determine the FTF is reliable. In the approach, a combination of an FTF with a band stop approach and a network modeling approach was applied. The method provides a good match between experimentally observed behavior and an analytical approach and can be used for instability analysis.

Keywords: combustion; instability; flame transfer function; thermoacoustic



Citation: Kapucu, M.; Kok, J.B.W.; Pozarlik, A.K. Experimental Investigation of Thermoacoustics and High-Frequency Combustion Dynamics with Band Stop Characteristics in a Pressurized Combustor. *Energies* **2024**, *17*, 1680. <https://doi.org/10.3390/en17071680>

Academic Editors: Marina Braun-Unkhoff and Sandra Richter

Received: 5 March 2024

Revised: 27 March 2024

Accepted: 28 March 2024

Published: 1 April 2024



Copyright: © 2024 by the authors. Licensee MDPI, Basel, Switzerland. This article is an open access article distributed under the terms and conditions of the Creative Commons Attribution (CC BY) license (<https://creativecommons.org/licenses/by/4.0/>).

1. Introduction

Gas turbine engine manufacturers and users are faced with the necessity to minimize: (i) nitric oxide emissions, (ii) variations in flue gas temperature in the combustor, (iii) combustor pressure drop, and maximizing the turbine inlet temperature. On top of these, for optimal and reliable operation of the gas turbine engine, the thermoacoustic instability should be avoided. These optimizations may be conflicting but it is very necessary to protect the engine, especially with respect to flue gas temperature variations and pressure oscillations. This becomes even more important now, when gas turbine engines are faced with a wide diversity of gaseous fuels of fossil resources or sustainable resources. This paper focuses on a design tool to predict the thermoacoustic instabilities for a specific design, fuel composition, and operating conditions. The interaction between acoustic wave propagation and the oscillation rate of heat release builds a feedback loop that causes a growth in amplitude of pressure oscillations over time. The prediction of this amplitude and the oscillation frequency are important to engine designers and operators, as the structural integrity of the engine is influenced by the acoustic pressure oscillations. This can have impacts on the design of the liner and burner.

The flame transfer function (FTF) describes the dynamic relationship between flow oscillations upstream of the burner and the response of the rate of heat release. The FTF is the active element in an acoustic network model, assuming one-dimensional acoustic propagation and a flame compact to the acoustic wavelength. In the field of thermoacoustics, the FTF has been studied extensively (see for examples the research of Cabot et al. [1] for a

stable flame and Paschereit et al. [2] for an unstable flame). However, most work has been completed for atmospheric combustion. Van Kampen and Kok [3,4] presented a method to measure the FTF at an elevated pressure with the use of pressure transducers and CFD-based FTF calculations. The FTF was obtained by Pozarlik [5] for various combustion chamber geometries. Significant activity was present between 420 and 450 Hz and maybe even beyond, according to previous investigations conducted in the same test unit [3–5]. This higher frequency activity is also present for a blend of H₂, which was observed by Pater [6], although this was in non-premixed combustion. Therefore, an improved device (a siren unit) was developed that can excite the system to higher frequencies (up to 600 Hz) and also at an elevated pressure. The scientific purpose and novelty of this study is to introduce an approach that is able to determine the FTF under pressurized conditions, contrasting with the existing literature where the FTF is mainly determined under atmospheric conditions.

The one-dimensional acoustic network model is a valuable tool for addressing stability issues of combustion systems. It has been widely used in the literature to address combustion instabilities [7–13]. Merk [7] investigated combustion instabilities of premixed gases by introducing a transfer matrix for laminar flames. Heckl [8] studied the acoustic field in a Rijke tube by the inhomogeneous wave equation with a monopole-type source term. Dowling [9] used a simple duct with no mean flow and one end closed and one end open. Unsteady heat release coupled with its code and frequency of the oscillations were then predicted. Schuermans et al. [10] applied a network-modeling approach to a gas turbine combustor with premixed, turbulent, swirler-stabilized flames in atmospheric conditions. Gentemann et al. [11] described a procedure for the estimation of acoustic transfer matrices of sudden area change in ducts by means of CFD analysis. Kopitz et al. [12] proposed a hybrid method combining CFD and low-order modeling. They link unsteady flow simulations with low-order modeling. They further explained the Nyquist stability criterion and its adaptation to thermoacoustic instabilities. Lecture notes of Polifke [13] provides a detailed explanation to system modeling and stability analysis. The computational effort for the network model is far less than that of the use of a three-dimensional compressible flow solver, and hence it can be applied to assess the effect of design or operation variations in acoustic systems. Input parameters, such as adequate acoustic boundary conditions and coupling of the dynamic flame behavior in the form of the flame transfer function, are very crucial for the acoustic network model's accuracy. The interaction of the acoustic waves with the flame and geometry is very complex. Therefore, these input parameters are not easy to calculate using first principles. For this purpose, accurate flame transfer functions (FTF) and well-defined boundary conditions need to be introduced into the model.

An acoustic transfer matrix can be constructed in a number of ways. Van der Eerden [14] established relations between the mass flow perturbations and the total pressure wave amplitudes. Instead of using the total pressure wave amplitudes, Hubbard and Dowling [15] use the forward-travelling wave and backward-travelling wave, called Riemann invariants. The scattering formulations are the other method developed and used by authors like Polifke [16] and Hobson [17]. The scattering matrix formulations provide a transfer matrix between pressure and velocity fluctuations. The method suggested by Van der Eerden has an advantage since this formulation uses the amplitude of the whole pressure wave, which is obtained from pressure transducers directly during measurement. Consequently, the experimental observations may be readily compared to the model.

In this paper, Section 2 provides a comprehensive description of the experimental setup with its sensors and diagnostic equipment. The background of the FTF measurement technique is described in Section 3. Additionally, the fuel excitation system is also explained in detail. The measured data for the FTF are shown in Section 4. Here, a comparison of the pressure spectrum at a certain location in the combustion chamber is also made between measurement and simulation. The measured FTF is then coupled with the one-dimensional acoustic network model for a stability analysis. The proposed method to measure FTF using Siren and pressure transducers proves to be unique, by allowing FTF

measurements in a pressurized combustor. The combustor stability prediction and data correlation by application of the n - τ - σ correlation is investigated and improved data fits are proposed.

2. Experimental Setup

The experimental investigation was performed on a pressurized single burner test rig, which was designed to provide, at lab scale, the conditions representative for full-scale gas turbine combustion chambers with a view of the thermal power density, pressure, and inlet air temperature. The combustor length was made much larger than the gas turbine combustors (1.8 m) to avoid acoustic coupling to the combustion dynamics. The setup can operate at 500 kW thermal power at 5 bar absolute pressure. The test rig major components are combustion air, cooling air and a fuel supply system, the plenum, the burner, the combustion chamber, and a throttle valve for the control of pressure. In Figure 1, the rig setup is shown in axial cross-section. The setup is equipped with dynamic (“P”) and static (“Ps”) pressure sensors respectively, thermocouples (“T”), and the photomultiplier tube (“PMT”) for chemiluminescence measurements. Figure 1 is explained in more detail in reference [4,5].

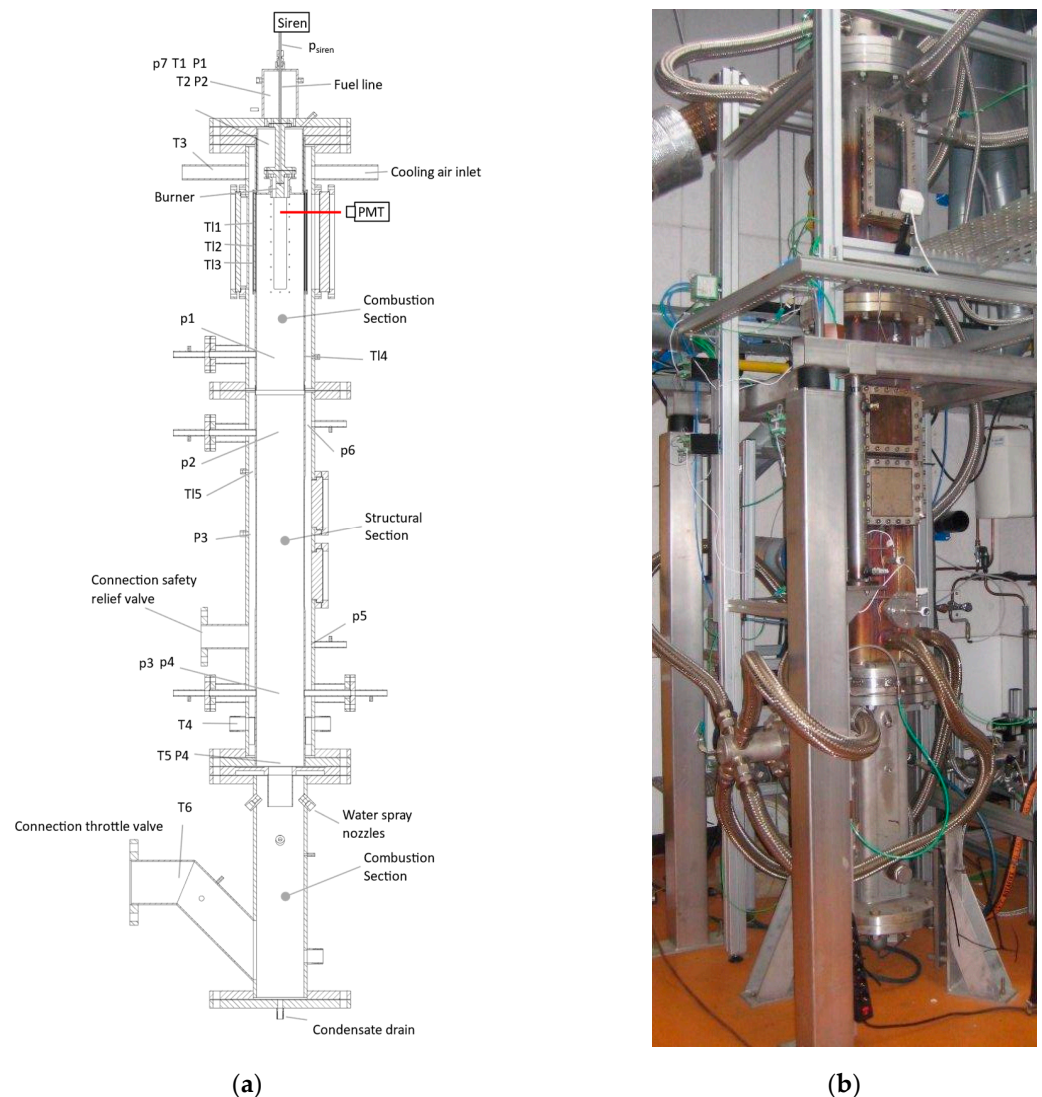


Figure 1. (a) Experimental setup drawing [4], (b) original picture of the experimental setup.

2.1. The Plenum and the Burner

The preheated air flows into a plenum. The introduction of the preheated air is performed by a total of twelve 7-mm-diameter holes. The plenum is designed as an acoustic decoupler. These holes introduce a large area change, significant pressure drop, and high velocity. The plenum feeds air to the burner. The burner has radial swirler vanes, inducing a swirling airflow with a swirl number of around 0.7. The central hub of the burner hosts four fuel nozzles. Natural gas is introduced from these nozzles into the swirled air flow. Acoustic feedback into the fuel line is avoided thanks to very high velocities in the fuel nozzles (Mach number = 0.8). The fuel nozzles inject high-velocity jets in the air flow annulus, achieving a technically premixed combustible air/natural gas flow at the burner annulus exit flow [4].

The combustor is built of a square cross-section SS316 pressure casing enveloping a 4-mm-thick SS 310 ($150 \times 150 \text{ mm}^2$) combustor lining. Between the liner and the pressure casing, a cooling airflow is introduced to decrease the temperature and thermal stress of the structural parts. Different from a gas turbine engine, the cooling airflow is controlled separately from the combustion airflow. What is also different, is that there is not an open connection between the cooling and combustion airflows. These arrangements are all provided to ensure optimal, controlled acoustic conditions for the flame transfer function measurement and input parameters for acoustic network modeling. The liner has an internal length of 1813 mm, with an upstream opening for the burner mouth and a downstream opening to the flue gas outlet. The combustion takes place in this liner duct. Preheated air at 300 °C enters the burner from a plenum. In-between the upstream plenum and the combustion chamber, a flame shield cooled by the input airflow is located. A spark plug is used for ignition. The presence of the flame is checked optically via quartz glass windows.

The combustor flue gases exit through an end flange with flow contraction (a reduction in the flow cross-section to about 25%). This contraction at the exit of the combustion chamber forces a significant share of the acoustic wave energy to reflect back into the combustion chamber. In the cooling section of the setup, hot flue gasses from the combustion chamber are mixed with cooling air from the liner. In order to prevent any damage to the throttle valve, the flue gas temperature could be further reduced by a water spray.

2.2. Air and Fuel Supply System

The pressurized air is provided by a dual-screw compressor and intercooler with a 10-bar pressure supply. The compressor feeds separate lines for the combustion airflow and cooling airflow. Similarly, the natural gas is also supplied by a combination of a screw compressor and intercooler at a 10-bar gauge. Bronckhorst mass flow controllers are used to control for both air (2 piece) and fuel (1 piece) flow. These are all calibrated and every mass flow controller has a 1% accuracy at maximum scale. All connecting ducts of the setup and the supply lines are chosen in such a way that the Mach number remains below 0.3. Thus, keeping the velocities under this value avoids flow noise in the supply line [18].

The flow from the compressors passes through several filters to clean the gas or air prior to entering the mass flow controller valves. It is important to keep the air and gas quality ideal during experiments. The natural gas flows through a special filter to remove any possible water content. The compressed air is first cooled by an intercooler and right after, it is dried by a dryer. In a gas turbine engine, the compressor section of a gas turbine provides pressurized and preheated air. This thermal compressor effect is simulated here by passing the combustion air downstream of the mass flow controller valve through a 120 kW electrical preheater prior to entering the combustor. The heater has the capacity to heat 360 g/s of air from room temperature to 300 °C.

2.3. Diagnostic Equipment

Various sensors are used to monitor and collect data during measurements. The acoustic pressure is measured using Kulite piezoelectric pressure transducers (XTE 190M).

These pressure sensors can measure 0 to 0.35 bar acoustic pressure. To avoid exposure of the Kulites to temperatures above 175 °C, the pressure transducers are mounted on acoustic transmission tubes situated on the combustor casing as seen in Figure 2. The transducers' temperature is further reduced by means of an external airflow over the Kulite sensors. These acoustic transmission tubes are connected to semi-infinite hoses, which are filled with acoustic damping material. Thus, the reflection of the acoustics is suppressed in the transmission tube.

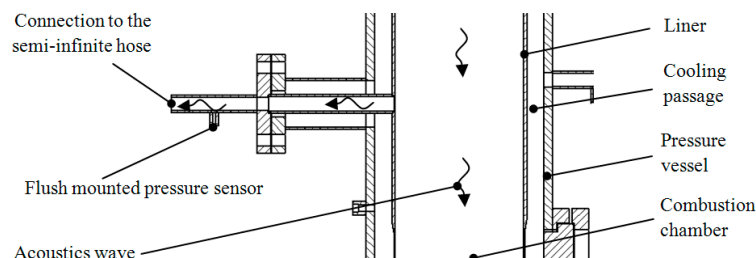


Figure 2. Pressure transducer connections [5].

The Kulite pressure transducers can be used at elevated pressures by equalizing the static pressure on both sides of the sensor diaphragm. A flexible, thin hose provides the reference pressure. The pressure inside the combustor is supplied by a relatively larger hose to a reference pressure supply station. Due to the viscothermal losses inside the thin hoses and volume of the reference pressure supply station, a Kulite sensor receives far less acoustic energy.

In order to increase the measurement accuracy, all pressure transducers are calibrated with respect to a reference sensor using a calibration tube. The relative amplitude and phase errors between the pressure transducers can be minimized with the calibration tube [19].

Temperature profiles of the setup and the flow from the inlet until the chimney are monitored by K-type thermocouples. Locations of the thermocouples are shown in Figure 1.

The heat release rate perturbation is the key parameter in the thermoacoustic problems. Measuring the heat release rate directly is not possible. However, earlier investigations in the literature showed that the heat release can be estimated using optical techniques. A well-known method to obtain the heat release is by integrating the chemiluminescence intensity of the intermediate chemical species (OH^* , CH^* , etc.). Among these intermediate chemical species, the OH^* chemiluminescence is a better indicator of the heat release rate and it is linearly dependent on the heat release rate [20,21].

In this study, the heat release rate fluctuations are measured via the OH^* chemiluminescence emitted from the flame, using a photomultiplier (Thorlabs amplified PMT) with a 308 nm wavelength UV filter. The experimental setup is equipped with quartz glass windows at the upstream end of the combustion chamber in both a liner and pressure casing. The size of the window is $120 \times 150 \text{ mm}^2$, which is large enough to see the whole flame. The PMT is positioned in front of this window.

2.4. Data Acquisition System

Data acquired in the experiments are processed by National Instruments' equipment [22]. Table 1 summarizes the hardware and parameter settings.

Table 1. DAQ hardware and parameter settings.

Input (12 channels)	NI9239
Output	NI9263
NI Compact DAQ Chassis	NI9188
Max sample rate	50 kS/s
Measurement sample rate	3125 S/s
Measurement duration	3.2 s (10,000 samples)

3. The Flame Transfer Function

This section presents the FTF measurement technique. When a disturbance is introduced to a combustion system, such as a change in pressure, sound waves, or equivalence ratio, the FTF measures how that input affects the rate of heat release. This is essential for gaining a grasp of and being able to accurately forecast combustion instability in a variety of systems, such as gas turbines.

For the flame transfer function measurements, it is necessary to have a flow excitation unit for gas or airflow or both. Loudspeakers are often observed as an excitation unit in atmospheric combustors. However, it is challenging to install a loudspeaker on a high-pressure combustor for safety and performance reasons, in view of the necessary back pressure. Some authors use a control valve for exciting the flow. This type of device has a somewhat lower maximum frequency of oscillation [4,5].

Another option is to use a siren-like excitation device, i.e., with a rotating part [23–26]. For the acoustic excitation of the fuel flow, a rotational speed-controlled siren is designed and placed at the beginning of the fuel line. The siren consists of one static and one rotating disc both having a special hole profile cut in them. The shapes of the holes are made in such a way that a sinusoidal excitation (wave form) is generated with sufficient amplitude and a large signal-to-noise ratio. The rotating disc has 15 holes and the static disc is cut with one hole. Details of the design can be seen in Figure 3.

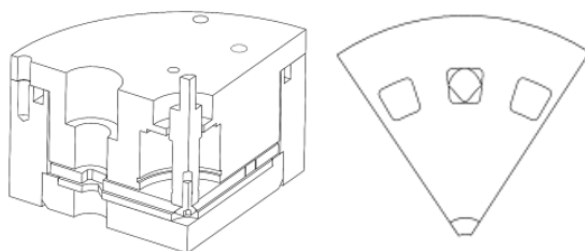


Figure 3. Siren CAD model (left); hole profiles (right).

The rotation of the siren shaft is driven by means of a variable RPM AC motor. The rotational speed is controlled by a frequency converter to provide stable frequencies. A reference signal for FTF measurements is provided by a pressure transducer downstream of the siren. Figure 4 show the siren performance at 500 Hz. Figure 4a demonstrates that the siren signal approaches a sinusoidal signal fairly well. Figure 4b shows the FTF of the time signal. There is a harmonic frequency induced by the siren at about -15 dB at twice the siren frequency, below the main induced signal of 156 dB at the 500 Hz siren frequency. Figure 5a shows the frequency variation in the siren performance at 500 Hz. The main frequency is between 499 and 501 Hz. Figure 5b presents the siren excitation performance on frequency range up to 600 Hz. It can be seen that a similar excitation can be delivered over the desired frequency range.

The FTF gives the correlation between the equivalence ratio fluctuations of the burner's exit conditions and the volume-integrated rate of heat release by the flame. Above, it has been explained how the mass flow perturbation of the fuel flow, as a function of an excitation unit, at the point of fuel injection can be measured. As an excitation unit, the in-house-developed siren system is used. The procedure to measure the FTF with the siren is described below. The FTF is defined in Equation (1):

$$H_f(\omega) = \frac{\overline{\dot{m}'_f} \cdot \dot{Q}'}{\overline{\dot{Q}} \cdot \dot{m}'_f} \quad (1)$$

where, $\overline{\dot{Q}}$ and \dot{Q}' represent the mean rate of heat release and its fluctuations, $\overline{\dot{m}'_f}$ and \dot{m}'_f represent the mean and perturbed mass flow, and ω is the frequency. The well-known

relation between the equivalence ratio fluctuations and mass flow fluctuations is discussed in references [3,4].

The mass flow fluctuations forcing the flame are reconstructed by using the pressure signals only. To this end, the FTF is factorized into several relatively simple-to-measure relations, as seen in Equation (2):

$$H_f = \frac{\overline{\dot{m}}_f}{\overline{\dot{Q}}} \cdot \frac{\dot{Q}'}{\dot{m}'_f} = \frac{\overline{\dot{m}}_f}{\overline{\dot{Q}}} \left[\frac{\dot{Q}'}{p'_{siren}} \cdot \frac{p'_{siren}}{\dot{m}'_f} \right] \quad (2)$$

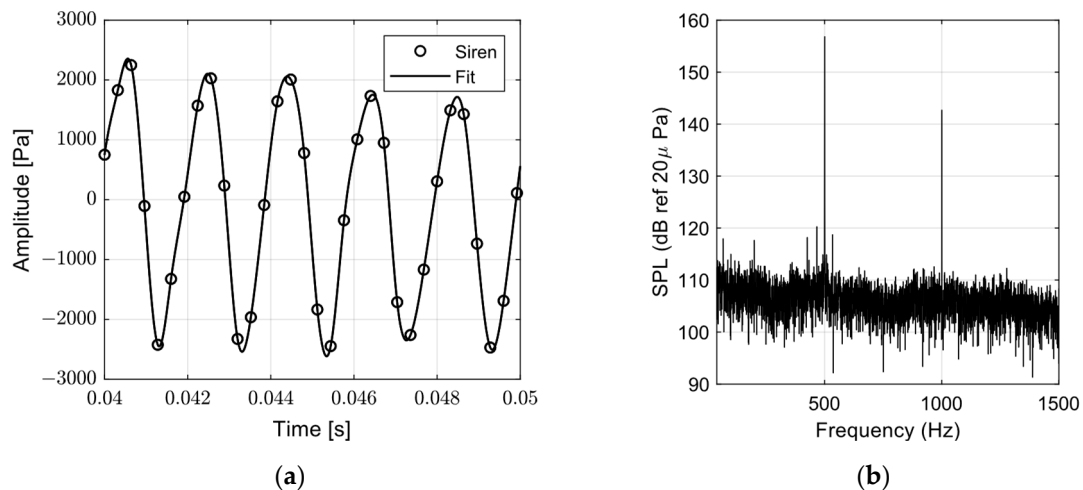


Figure 4. Siren performance at 500 Hz (a) time signal with polyline fit (b) FTF of the time signal in sound pressure level (SPL).

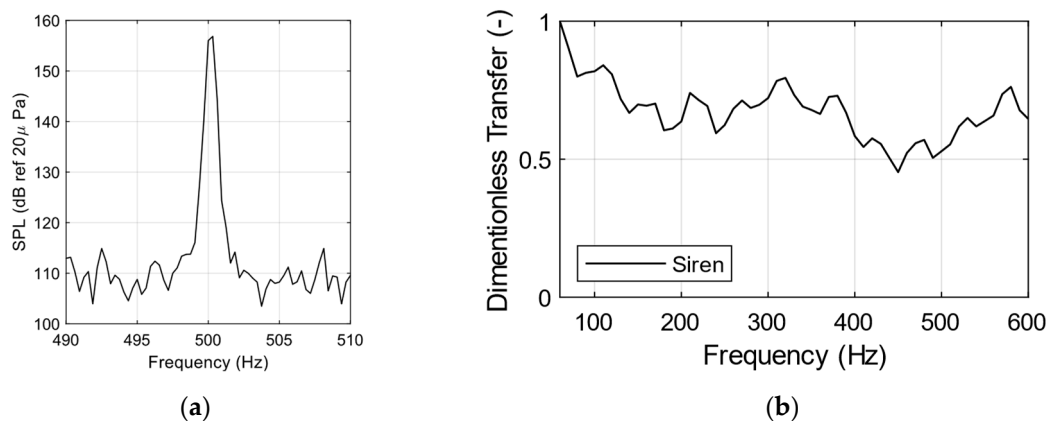


Figure 5. The excitation performance of the siren. (a) Frequency variation performance. (b) Frequency excitation range performance.

Figure 6 provides a concise summary of the procedure for measuring the FTF.

The siren is positioned directly on the fuel supply line at a point where it is closest to the fuel supply nozzles in the burner. The distance between the siren and the fuel supply nozzles is approximately 0.7 m. This length causes a phase shift and amplitude variation at the fuel nozzle exits relative to the mass flow fluctuations at the siren exit plane. Measuring the fuel mass flow fluctuations at the nozzle exit is not possible due to a lack of access. A 1:1 scale experimental model of the fuel supply (see Figure 7) was used in order to determine the correlation between the fluctuations at nozzle and siren exit. By employing a quasi-1D steady acoustic approach, the velocity fluctuation at the fuel nozzles is converted from the measured pressure upstream of the nozzle [27]. This method is discussed more in detail in the references [3,4,27].

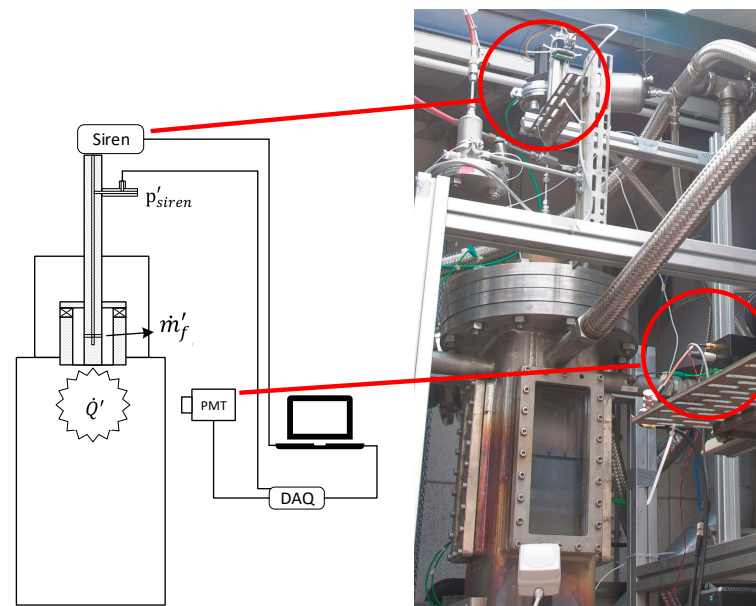


Figure 6. Overview of FTF measurement method.

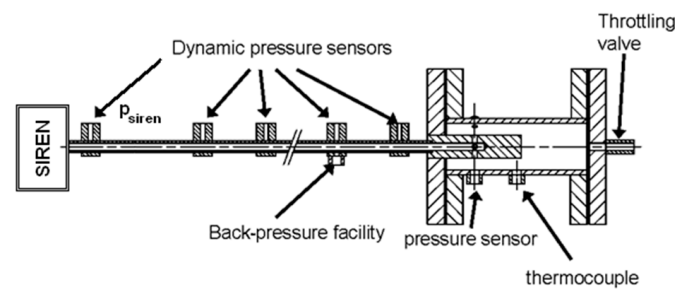


Figure 7. Cross-section view of the real-scale experimental model of the fuel supply line.

The transfer function is given by the correlation between the mass flow fluctuation \dot{m}'_f at the fuel nozzle exits and the pressure oscillation measured downstream of the fuel nozzle in the calibration device shown in Figure 7:

$$\dot{m}'_f(\omega) = \frac{Vi\omega}{c_0^2} p' \quad (3)$$

where ω is radial frequency, V is volume, c_0 is the speed of sound, and p is pressure.

During an FTF measurement, the fuel supply line pressure signal serves as a reference signal to correlate the siren induced mass flow perturbations. Figure 8 shows the transfer function between the pressure signal of the siren (p'_{siren}) at the fuel supply line and the fuel nozzle mass flow fluctuation for two mass flow rates equivalent to thermal powers of 125 kW and 250 kW at respective absolute pressures of 1.5 and 3 bar. In these settings, the volume flow rate and equivalence ratio have been kept constant. An early version of these results was presented by Kapucu et al. [27].

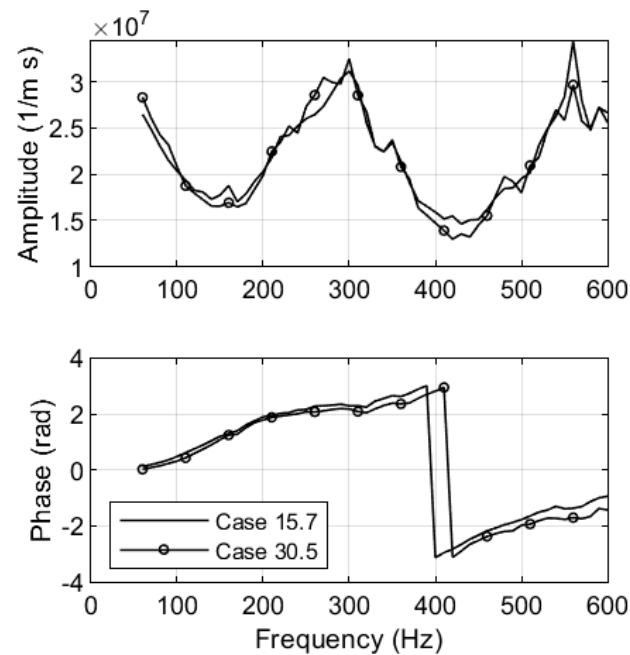


Figure 8. The amplitude (**top**) and phase (**bottom**) of the transfer function $\frac{p'_{siren}}{m'_f}$ for operation points 15.7 (125 kW at 1.5 bar pressure) and 30.5 (250 kW at 3 bar pressure).

It can be observed in Figure 8 that the amplitude and phase spectra are almost identical for the two power/pressure settings. This can be explained by the fact that the time mean velocities in the combustor were kept constant. The ratio of the pressure transducer signal amplitude to forced mass flow oscillation varies between 1.5 at 175 Hz and 425 Hz to about 3 at 300 Hz and 550 Hz. Both cases exhibit a steady and identical slope as the frequency increases, indicating an almost linear relationship between the phase shift of the siren pressure signal and mass flow fluctuations at the fuel nozzle per unit time. On the basis of a constant time delay, the convective time delay can be estimated as 1.44 ms for the 15.7 case (125 kW at 1.5 bar), whereas for the 30.5 case (250 kW at 3 bar), it is 1.41 ms. This difference is within the measurement error. These results show that the siren method provides accurate time delay measurements in two different power settings at equal volume rates.

It is important to have an acoustically stable system for the FTF measurements. It is desired to have a non-reflective end condition at the boundaries so the reflective waves cannot amplify the system's eigenfrequencies. For our application, this criterion is met only to some extent, for the reason of the need to use a throttle valve for pressure control. It can be shown however, that the excited combustion dynamics are dominant over any kind of eigenfrequency of the setup. This can be seen in Figure 9. This figure shows the measured pressure spectra of the setup at 125 kW thermal power at 1.5 bar. The amplitudes of the acoustic eigenfrequencies are relatively low, meaning that the spontaneous oscillations are well damped and the combustion dynamics is the major driving process for the acoustics. It would still be beneficial to correct the flame transfer function using the spontaneous oscillations of the system. In Figure 10, the comparison of the PMT signal with and without excitation is presented. When the system is excited, the PMT signal increases with almost a constant offset. However, when the excitation frequency matches with the systems eigenfrequency, it amplifies the signal.

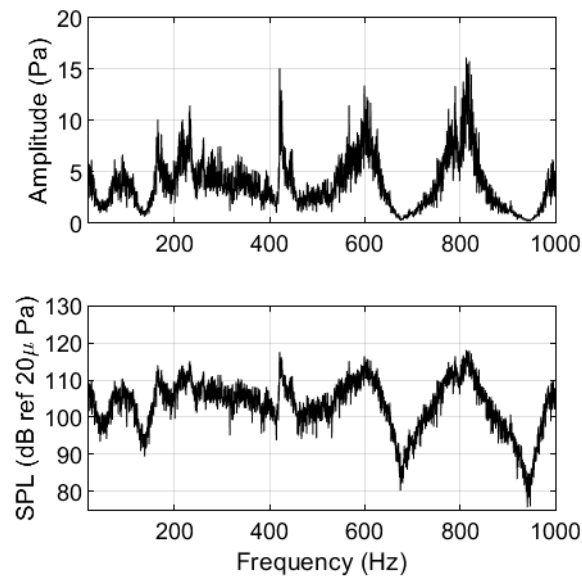


Figure 9. Measured p1 pressure spectrum at 125 kW at 1.5 bar. The **(top)** figure is amplitude in Pa and the **(bottom)** figure is the amplitude in SPL.

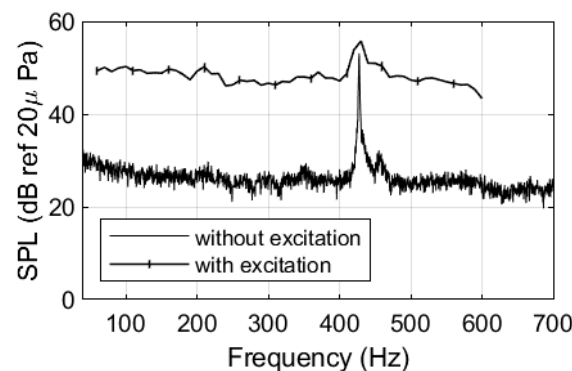


Figure 10. PMT signal with and without excitation.

Correlation of the Fits

The measured FTF provides information about the flame dynamics for a certain range of frequencies. In order to correctly implement the FTF in the network model system, the FTF needs to be represented in the complex frequency domain. There are two types of methods introduced in the literature to present the FTF in a complex plane. One is to use a theoretical model that is rather complicated because it depends on large numbers of parameters such as the fuel, the flow settings, the type of flame, etc. The second method is based on intentionality of the measured FTF. In other words, this means using a model to fit the measured FTF data. There are models available for specific flames and application areas. In this work, the flame is premixed and a swirl-type burner is stabilized, which leads us to relevant flame models. The more extensive discussion on flame models can be found in the work of Kornilov [28] and Hoeijmakers [29]. The FTF can be represented by time lag models such as the well-known $n - \tau - \sigma$ model.

$$H_f(\omega) = ne^{-i\omega\tau}e^{-\frac{1}{2}\omega^2\sigma^2} \quad (4)$$

In this equation, n is the amplification factor, τ is the time delay, and σ is the time delay distribution. The model provides an FTF function with a low-pass filter behavior that is characteristic for many experimental observations [30].

Using the $n - \tau - \sigma$ model to describe a flame provides a good match with the phase of the FTF but not with the magnitude of the FTF. Another approach would be to use a

rational transfer function model that is common in control systems and very well capable of capturing the response of a wide range of dynamical systems [12]. The rational transfer function is usually defined as a fraction of polynomials:

$$H_f(s) = \frac{P_N(s)}{P_D(s)} = \frac{a_n s^n + \dots + a_0}{b_m s^m + \dots + b_0} \quad (5)$$

where N and D are the order of the nominator and denominator, respectively. The performance of the $n - \tau - \sigma$ model and the rational transfer function model is compared in the next section using the experimental results.

4. FTF and Stability Results

Figure 11 shows the measured FTF for different operating points. The measured gain and phase plots at 125 kW and 250 kW are almost identical. The gain is around unity between 50 Hz and 300 Hz, with a local maximum at 150 Hz. The gain increases to about 2 at two peaks at 430 Hz and 460 Hz and decreases subsequently with frequency. The phase decreases linearly with frequency and with equal slope at both 125 Hz and 250 kW. This indicates that the system performance does not change with a change in pressure conditions, provided that the velocity is kept constant.

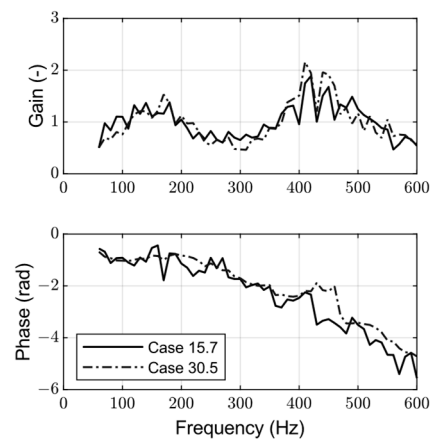


Figure 11. Comparison of FTF measurements for different operating points. Case 15.7–125 kW at 1.5 bar (—), Case 30.5–250 kW at 3 bar (---).

In order to perform a stability analysis with the use of a one-dimensional network model, the measured flame transfer function, with data on discrete frequencies, is projected in the $n - \tau - \sigma$ model, Equation (3), and the rational transfer function, Equation (4).

The performance of the $n - \tau - \sigma$ model and rational transfer function model is depicted in Figure 12. The $n - \tau - \sigma$ model exhibits low-pass filter behavior for the magnitude part of the FTF and constant time delay. In view of the low-pass behavior, it is not capable of capturing the features of the magnitude measurements, which show magnitude peaks at several frequencies. The rational transfer function method shows a very good performance mimicking the dynamics in both magnitude and phase behavior of the data. Yet, the model response of the rational transfer function is highly dependent on the order of the nominator and denominator. Having the best fit for the data might introduce instability to the function. Therefore, it requires extra attention to determine the orders. A more detailed discussion about the performance of the rational function can be found in the work of Hoeijmakers [29]. The rational transfer function parameter settings used for the results shown in Figure 12 provide satisfactory results and are specified in full in Appendix A.

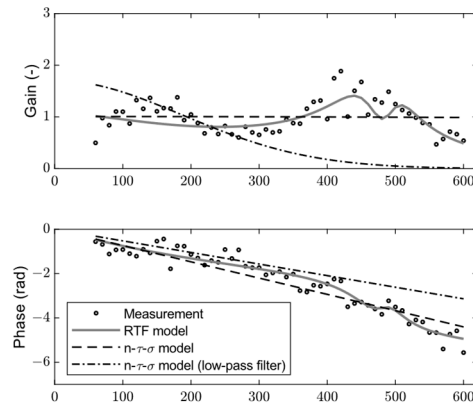


Figure 12. The frequency response of the flame models. Measurement (o), $n - \tau - \sigma$ model (---) with $n = 1, \tau = 1.168 \times 10^{-3}, \sigma = 0.045 \times 10^{-3}$; $n - \tau - \sigma$ model (—) with $n = 1.705, \tau = 0.83244 \times 10^{-3}, \sigma = 0.84745 \times 10^{-3}$; rational transfer function (RTF) method (—), (PN = 5, PD = 6). (Parameters are presented in Appendix A).

Using the network model, we break down the test rig into its component parts. The plenum, air-line, fuel-line, flame, and combustion chamber are all components of the model used in this investigation. For the purpose of pressure calculation, an extra node is positioned within the combustion chamber. In the combustion chamber, a linear distribution of temperatures is used. The network model’s boundary conditions and input parameters are displayed in Table 2.

Table 2. Parameters for acoustic network model.

Power	125 kW
Pressure	1.5 bar
Air temperature	573 K
Adiabatic flame temperature	1811 K
Flue outlet temperature	1125 K
Combustion chamber length	1813 mm
Distance of pressure sensor (P1)	406 mm
ζ_{up} and ζ_{siren}	Hard acoustic boundary
ζ_{down}	$ R \approx 0.7$

Table 3 presents the comparison of the measured and predicted eigenfrequencies. The eigenfrequencies can be also seen in the pressure spectrum measurement presented in Figure 9. The 4 resonant frequencies are very well predicted with the network model. This indicates both the added value of the network model, as well as the effect of the combustion dynamics on the system eigenfrequencies.

Table 3. Measured and predicted acoustic eigenfrequencies.

n	1	2	3	4
Frequency Measured [Hz]	232	421	604	815
Frequency Modeled [Hz]	240	424	616	820

Further, the one-dimensional acoustic network model can be used to predict instabilities when the $det(S) = 0$ for complex eigenfrequencies $\omega_r + i\omega_i$. Here, ω_r is the frequency of the oscillations and ω_i is the indication of the growth rate of the oscillations. When $\omega_i < 0$, the oscillation grows exponentially in time. The growth rate (GR) is defined as the ratio of the pulsation amplitude of two successive pulsation cycles [16,31] (see Equation (6)). Thus, fluctuations are amplified when the $GR > 0$ and damped for the $GR < 0$.

$$GR = e^{-2\pi \frac{\omega_i}{\omega_r}} - 1 \tag{6}$$

The modeled FTF function is implemented in the network model for the instability analysis. The results are presented in Figure 13, from which it could be noted that all the models predicted the first instability around 230 Hz. This is in the range of the first eigenfrequency of the system (see also Table 2). During the experiments, no combustion instability or elevated pressure amplitudes were observed at this frequency. The reason for this discrepancy might be the inaccuracy of the model at low frequencies.

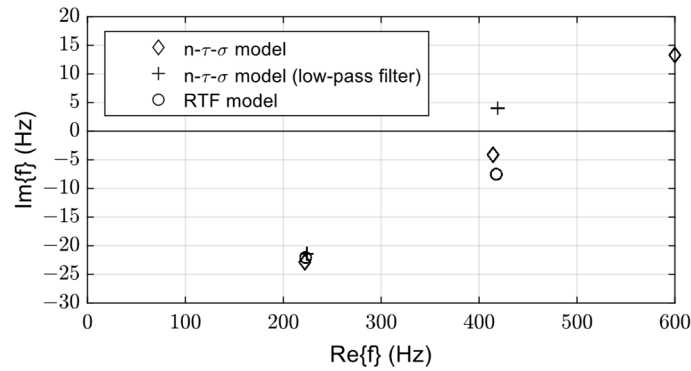


Figure 13. Instability analysis.

Based on the experimental data provided in Figures 9 and 10 and the model results, it can be concluded that the main activity is correctly located around 420–430 Hz. However, the rate of growth is too small to lead to high-amplitude, self-sustained oscillations. The FTF results obtained from the siren method are the most accurate with respect to predicted resonant frequencies and the growth rate of the instability.

In order to shed light on the discrepancy between observed and predicted instability at the low frequency range around 200 Hz, the sensitivity of the acoustic network model parameter settings to different values of the FTF gain and the exit reflection coefficient was investigated. The predicted growth rates of the eigenfrequencies are presented in Figure 14 at different parameter settings. The gain and the time constant of the phase shift of the FTF were kept constant as $n = 1$ and $\tau = 1.1686 \cdot 10^{-3}$ s respectively, and the exit reflection coefficient R was varied. The system is fully stable when $R < 0.4$. For $R > 0.4$ the growth rate is positive for both eigenfrequencies.

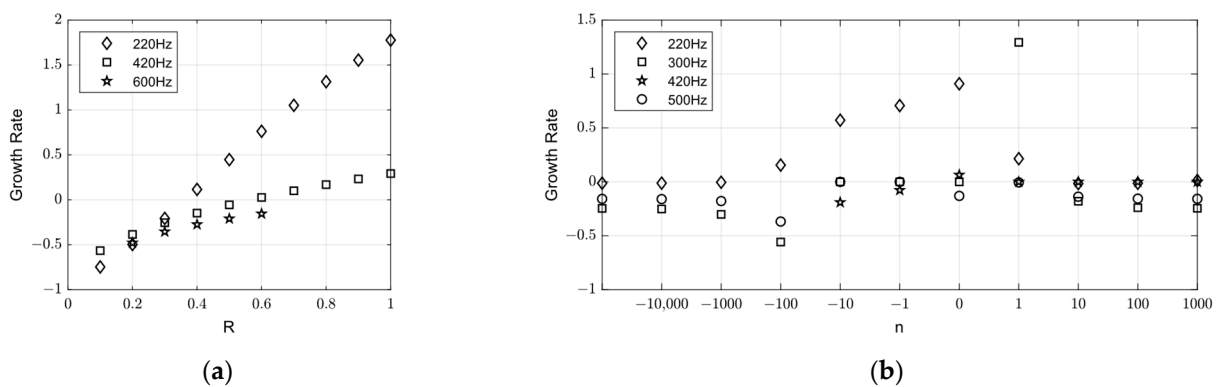


Figure 14. Found eigenfrequencies for different exit reflection coefficient (a) and different FTF gains (b).

Next, the growth rate of the instabilities for different values of the gain is explored. For this calculation, the time constant for the phase shift of the FTF and the exit reflection coefficient were kept constant as $\tau = 1.1686 \cdot 10^{-3}$ s and $R = 0.65$, respectively. For these values, when the gain is above 10 or below -10 , the system response changes. For these values, new eigenfrequencies are introduced. For the gain values between -10 and 10 , the system has similar eigenfrequencies as observed in the experiments. The growth rates of the

instabilities are positive for 220 Hz even though the amplification factor is negative. For the 420 Hz frequency, the growth rate changes from positive to negative with decreasing gain.

It can be concluded that for the low frequencies, the exit impedances have more influence on the instability than the amplification factor. For high frequencies, this is the combination of both the acoustics and flame dynamics that are affecting the instability. Returning to the discrepancy between predicted and observed system instability at a low frequency, it can be concluded that the main cause is an incorrect value of the parameter setting of the exit impedance. The FTF model data are likely to be accurate and not responsible for the mismatch.

5. Conclusions

Combustion dynamics in a pressurized combustor burning natural gas and preheated air are investigated in this paper. The experimental determination of the flame transfer function (FTF) is carried out at 1.5 bar and 3 bar. Our investigation concludes that the FTF demonstrates characteristics that deviate from the typical low-pass behavior. This is one of the novelties of the present work. The $n - \tau - \sigma$ model appears inadequate in capturing these unique characteristics of the FTF. Therefore, an alternative model is suggested to effectively capture these features. On the basis of the measured data, an acoustic stability analysis is performed. Boundary conditions play a critical role in accurately predicting instability.

Interestingly, the FTF of the swirler-type burner designed for premixed natural gas and air does not have a low-pass behavior but also exhibits amplification at higher frequencies, after a local minimum amplification at 300 Hz. To capture this behavior, the flame transfer function is determined with a method based on siren excitation and by applying fuel-line pressure transducer data to determine the fuel mass flow oscillations. This is another novelty of the work. The siren can provide fuel flow oscillation up to 600 Hz. The 1.5 and 3 bar pressure test cases compare very well for the FTF amplitude as a function of frequency. For the phase shift, measurements indicate a constant but slightly varying time delay with pressure (1.31 ms. for 1.5 bar and 1.09 ms. for 3 bar operations, respectively).

The measured discrete data points are matched with a fitted continuous function. This function is implanted in the acoustic network model for stability analysis. A comparison is made between FTF fits for the n - τ - σ and the rational transfer function methods. It appears that for the present data, the rational transfer function performs well, as the FTF does not have a low-pass but a band-pass behavior. An extensive analysis and discussion of the simulated and measured pressure spectra at a selected location is provided. The simulated and observed eigenfrequencies of pressure oscillations agree very well. The predicted growth rates of the instabilities are calculated. The acoustic network model correctly predicts a small net growth rate at 424 Hz but overpredicts the growth rate at 221 Hz.

In order to establish the cause of the discrepancy in the growth rate at 221 Hz, a parameter sensitivity analysis for the gain amplitude and time constant of the FTF, as well as the value of the exit acoustic reflection, has been performed. It shows that the prediction relies on the exit impedance parameter setting. For the reliable design and operation of combustion systems, the application of a thermoacoustic analysis method as demonstrated in this work is a useful and effective tool. It can provide valuable information regarding the thermoacoustic instabilities and frequencies at which they may appear. This study primarily centered on natural gas as a fuel, but the knowledge and insights acquired are applicable to the combustion of various fuel gases, including hydrogen. It is noteworthy that the FTF band stop approach is probably even more important for hydrogen than methane, as it is known based on the literature that hydrogen flames have more thermoacoustic activity at higher frequencies.

Author Contributions: Validation, M.K.; investigation, M.K.; writing—original draft, M.K.; supervision, J.B.W.K.; writing—review and editing, A.K.P.; writing—review and editing. All authors have read and agreed to the published version of the manuscript.

Funding: This research was funded by EC in the Marie Curie Actions Networks for Initial training, Project LIMOUSINE with project number [214905].

Data Availability Statement: The data presented in this study are available from 10.4121/40a460f0-b5df-4301-9a8f-1250754c7bb3.

Conflicts of Interest: The authors declare no conflicts of interest.

Appendix A

$$HF_{Siren} = \frac{\omega^5 a_1 - \omega^4 a_2 - \omega^3 a_3 - \omega^2 a_4 + \omega a_5 + a_6}{-\omega^6 + \omega^5 b_1 + \omega^4 b_2 - \omega^3 b_3 - \omega^2 b_4 + \omega b_5 + b_6} \quad (A1)$$

Table A1. Parameters of the rational transfer function model.

a_1	254.23 i	b_1	6431.017548392937897006049752 i
a_2	1084551.95	b_2	28143683.5938770174980163574
a_3	1046987085.12 i	b_3	114061616334.2061920166 i
a_4	33488605017316.56	b_4	214974463797900.625
a_5	352954545271784 i	b_5	492411166094701952 i
a_6	406601584529901289472	b_6	382766879396415733760

Table A2. Parameters of $n - \tau - \sigma$ Model.

	n	τ	σ
Full Frequency range	1.0052	1.1686 ms	0.0521 ms
Up to 270 Hz	1.705	0.83244 ms	0.84745 ms

References

- Cabot, G.; Vauchelles, D.; Taupin, B.; Boukhalfa, A. Experimental study of lean premixed turbulent combustion in a scale gas turbine chamber. *Exp. Therm. Fluid Sci.* **2004**, *28*, 683–690. [\[CrossRef\]](#)
- Paschereit, C.O.; Schuermans, B.; Polifke, W.; Mattson, O. Measurement of transfer matrices and source terms of premixed flames. *J. Eng. Gas Turbines Power* **2002**, *124*, 239–247. [\[CrossRef\]](#)
- Van Kampen, J.; Kok, J.B.W. Characterization of interaction between combustion dynamics and equivalence ratio oscillations in a pressurized combustor. *Int. J. Spray Combust. Dyn.* **2010**, *2*, 219–252. [\[CrossRef\]](#)
- Van Kampen, J.F. Acoustic Pressure Oscillations Induced by Confined Premixed Natural Gas Flames. Ph.D. Thesis, University of Twente, Enschede, The Netherlands, 2006.
- Pozarlik, A.K. Vibro-Acoustical Instabilities Induced by Combustion Dynamics in Gas Turbine Combustors. Ph.D. Thesis, University of Twente, Enschede, The Netherlands, 2010.
- Pater, S. Acoustics of Turbulent Non-Premixed Syngas Combustion. Ph.D. Thesis, University of Twente, Enschede, The Netherlands, 2007.
- Merk, H. An analysis of unstable combustion of premixed gases. In *Symposium (International) on Combustion*; Elsevier: Amsterdam, The Netherlands, 1957; pp. 500–512.
- Heckl, M.A. Active control of the noise from a Rijke tube. *J. Sound Vib.* **1988**, *124*, 117–133. [\[CrossRef\]](#)
- Dowling, A.P. The calculation of thermoacoustic oscillations. *J. Sound Vib.* **1995**, *180*, 557–581. [\[CrossRef\]](#)
- Schuermans, B.B.; Polifke, W.; Paschereit, C.O.; van der Linden, J.H. Prediction of acoustic pressure spectra in combustion systems using swirl stabilized gas turbine burners. In Proceedings of the ASME Turbo Expo 2000: Power for Land, Sea, and Air, Munich, Germany, 8–11 May 2000; p. V002T002A025.
- Gentemann, A.; Fischer, A.; Evesque, S.; Polifke, W. Acoustic transfer matrix reconstruction and analysis for ducts with sudden change of area. In Proceedings of the 9th AIAA/CEAS Aeroacoustics Conference and Exhibit, Hilton Head, SC, USA, 12–14 May 2003.
- Kopitz, J.; Polifke, W. CFD-based application of the Nyquist criterion to thermo-acoustic instabilities. *J. Comput. Phys.* **2008**, *227*, 6754–6778. [\[CrossRef\]](#)
- Polifke, W. System modelling and stability analysis. *Lect. Ser.-Von Karman Inst. Fluid Dyn.* **2007**, *9*, 7.
- Van der Eerden, F. Noise Reduction with Coupled Prismatic Tubes. Ph.D. Thesis, University of Twente, Enschede, The Netherlands, 2000.

15. Hubbard, S.; Dowling, A.P. Acoustic Resonances of an Industrial Gas Turbine Combustion System. *J. Eng. Gas Turbines Power* **2000**, *123*, 766–773. [[CrossRef](#)]
16. Polifke, W.; Poncet, A.; Paschereit, C.O.; Dobbeling, K. Reconstruction of acoustic transfer matrices by instationary computational fluid dynamics. *J. Sound Vib.* **2001**, *245*, 483–510. [[CrossRef](#)]
17. Hobson, D.E.; Fackrell, J.E.; Hewitt, G. Combustion instabilities in industrial gas turbines—Measurements on operating plant and thermoacoustic modeling. *J. Eng. Gas Turbines Power* **2000**, *122*, 420–428. [[CrossRef](#)]
18. Rayleigh, L. *The Theory of Sound*; Macmillan and Co.: London, UK, 1896; Volume 2.
19. Kapucu, M.; Kok, J. Acoustic Design Parameter Change of a Pressurized Combustor Leading to Limit Cycle Oscillations. *Energies* **2023**; *Submitted*.
20. Haber, L.; Vandsburger, U.; Saunders, W.; Khanna, V. *An Experimental Examination of the Relationship between Chemiluminescent Light Emissions and Heat-Release Rate under Non-Adiabatic Conditions*; DTIC Document: Los Angeles, CA, USA, 2001.
21. Price, R.; Hurle, I.; Sugden, T. Optical studies of the generation of noise in turbulent flames. In *Symposium (International) on Combustion*; Elsevier: Amsterdam, The Netherlands, 1969; pp. 1093–1102.
22. Instrument, N.C. *LabVIEW User Manual*; National Instrument Corporate: Austin, TX, USA, 2003.
23. Richards, G.A.; Yip, M.J.; Robey, E.; Cowell, L.; Rawlins, D. Combustion Oscillation Control by Cyclic Fuel Injection. *J. Eng. Gas Turbines Power* **1997**, *119*, 340–343. [[CrossRef](#)]
24. Cheung, W.; Sims, G.; Coppelstone, R.; Tilston, J.; Wilson, C.; Stow, S.R.; Dowling, A.P. Measurement and analysis of flame transfer function in a sector combustor under high pressure conditions. In Proceedings of the ASME Turbo Expo 2003, Collocated with the 2003 International Joint Power Generation Conference, Atlanta, GA, USA, 16–19 June 2003; pp. 187–194.
25. Alemela, P.R. Measurement and Scaling of Acoustic Transfer Matrices of Premixed Swirl Flames. Ph.D. Thesis, Technische Universität München, Munich, Germany, 2009.
26. Gentemann, A.; Hirsch, C.; Kunze, K.; Kiesewetter, F.; Sattelmayer, T.; Polifke, W. Validation of flame transfer function reconstruction for perfectly premixed swirl flames. In Proceedings of the ASME Turbo Expo 2004: Power for Land, Sea, and Air, Vienna, Austria, 14–17 June 2004; pp. 501–510.
27. Kapucu, M.; Kok, J.B.W.; Alemela, P.R. Characterization of acoustic oscillations in fuel supply lines. In Proceedings of the ICSV18, 18th International Congress on Sound and Vibration, Rio De Janeiro, Brazil, 10–14 July 2011.
28. Kornilov, V. Experimental Research of Acoustically Perturbed Bunsen Flames. Ph.D. Thesis, Technische Universiteit Eindhoven, Eindhoven, The Netherlands, 2006.
29. Hoeijmakers, P.M. Flame-Acoustic Coupling in Combustion Instabilities. Ph.D. Thesis, Technische Universiteit Eindhoven, Eindhoven, The Netherlands, 2014.
30. Schuermans, B. Modeling and Control of Thermoacoustic Instabilities. Ph.D. Thesis, EPFL, Lausanne, Switzerland, 2003.
31. Sattelmayer, T.; Polifke, W. Assessment of methods for the computation of the linear stability of combustors. *Combust. Sci. Technol.* **2003**, *175*, 453–476. [[CrossRef](#)]

Disclaimer/Publisher’s Note: The statements, opinions and data contained in all publications are solely those of the individual author(s) and contributor(s) and not of MDPI and/or the editor(s). MDPI and/or the editor(s) disclaim responsibility for any injury to people or property resulting from any ideas, methods, instructions or products referred to in the content.